PHOTOPRODUCTION: TOTAL CROSS SECTIONS AND VECTOR MESONS

A. M. Eisner
University of California
Santa Barbara, California 93106

I. INTRODUCTION

I've been asked to report on work done in the Tagged Photon beam at Fermilab, and also to cover some related contributions from Cornell. Since its inception, Fermilab's Tagged Photon Laboratory (TPL) has seen three experimental setups. The first was the Fermilab-Santa Barbara-Toronto collaboration which, after some early ψ photoproduction measurements, settled into its main goal of precisely measuring the total cross sections for hadronic photoproduction on protons and nuclei. In the course of these measurements, results were also obtained for the photoproduction of ρ^0, ω and ϕ mesons.

The second setup was the Santa Cruz experiment to measure elastic Compton scattering, and, more generally, to study final state photons, π^0's, η's (in the 2γ mode), etc.

Finally, and most ambitiously, the Tagged Photon Spectrometer System recently installed - and in the midst of its initial tests - will be a tool for studying the details of final states.

Of these three projects, only the first has progressed to the point of physics results, so that most of this talk will deal with those measurements. In addition, I will report on some recent results on vector meson electroproduction carried out on the LAME detector at Cornell.

Processes induced by high-energy real or spacelike photons can be thought of in two ways. One approach emphasizes the "hadronic structure of photons": the photon undergoes a fluctuation to a hadronic state, which must interact with the target in order to materialize the hadrons in the final state. (This approach can be useful in studying hadronic interactions which may not be accessible with laboratory beams; it is intended that the Tagged Photon Spectrometer will be used in this manner to study charm, for example.) A second approach regards the photon as a pointlike probe to study the structure of a hadronic target. This is the domain of the parton model and short-distance QCD.

That these may really be complementary points of view, appropriate to different reference frames, has been emphasized by a number of people, including the review article by Bauer et al.[1] (Grammer and Sullivan[2] have demonstrated the resemblance of the pointlike terms of a particular parton model to the high mass sum of generalized vector meson dominance.) The photon structure picture is most appropriate to the target rest frame; especially when the time which a hadronic fluctuation survives in this frame,

$$\Delta t \approx \frac{2\nu}{M^2 - q^2} \qquad (1)$$

(for a photon of 4-momentum q and energy ν and a hadronic state of mass M), is larger than the time it takes to traverse the target. It is often convenient to classify photon processes according to the somewhat artificial division between the two points of view. In this spirit, all of the topics I will discuss have traditionally been dealt with in terms of the photon's hadronic structure and hadron-like behavior.

II. TOTAL PHOTOPRODUCTION CROSS SECTIONS

A. Hydrogen Measurements

Perhaps the strongest high-energy evidence for the hadron-like behavior of the photon comes from the high precision measurements made at TPL of the photon-proton total cross section (Fig. 1).[3] (These results were presented, although not in final form, at the 1977 DESY conference; everything else I will show postdates that conference.) It was known that below 20 GeV $\sigma_{\gamma p}$ falls in a manner similar to that of hadronic total cross sections. In fact, the energy dependence was well-approximated by an average of $\pi^+ p$ and $\pi^- p$ cross sections (as suggested by the idea of ρ-dominance), albeit 200 times smaller. The high energy γp data exhibit the characteristic behavior of hadrons in that new energy-range: a rising total cross section. A straight-line fit to the data at $E_\gamma \geq 35$ GeV has a slope $5\frac{1}{2}$ standard deviations from 0. The data have systematic uncertainties estimated to be 0.7%, of which 0.4% could be energy-dependent.

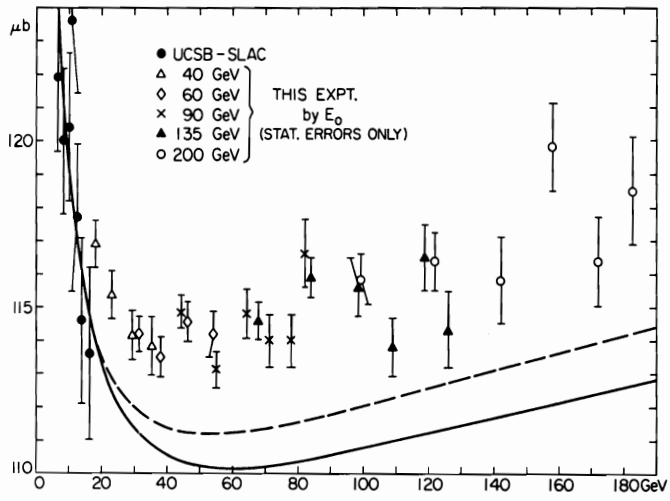

Fig. 1. The total hadronic photoproduction cross section from protons vs. photon energy (from Ref. 3, with low-energy points from Ref. 5). The curves are described in the text. E_o refers to the electron beam energy before tagging.

A general formulation of hadron-dominance for the elastic Compton amplitude (to which $\sigma_{\gamma p}$ is related) is shown in Fig. 2. H and H' are hadronic states with the quantum numbers of the photon. The high-mass sum may be redundant with a direct (pointlike) interaction. In the most general form of vector meson dominance (GVMD), this is written (for real photons) as

$$f_{\gamma p \to \gamma p} = \sum_{V,V'} \frac{e^2}{4\gamma_V \gamma_{V'}} f_{Vp \to V'p} \,. \qquad (2)$$

(At high E_γ, diffractive processes dominate, so one has no $\rho - \omega$ cross terms; there might, however, be some $\omega - \phi$ mixing.) For diagonal GVMD, this implies

$$\sigma_{\gamma p} = \sum_{V} \frac{e^2}{4\gamma_V^2} \sigma_{Vp} \qquad (3)$$

For the ρ^0, ω and ϕ, one has quark model relations:

$$\sigma_{\rho^0 p} = \sigma_{\omega p} = \frac{1}{2}(\sigma_{\pi^+ p} + \sigma_{\pi^- p})$$
$$\sigma_{\phi p} = \sigma_{K^+ p} + \sigma_{K^- p} - \sigma_{\pi^- p} \qquad (4)$$

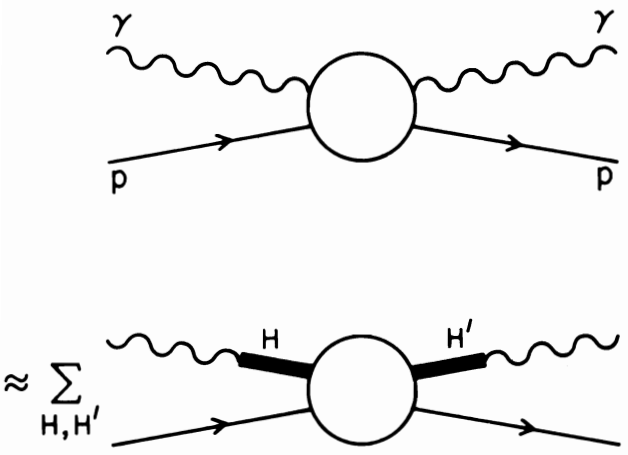

Fig. 2 Hadron dominance for the γp elastic amplitude.

The solid curve of Fig. 1 represents the sum of Eq. (3) for just these three mesons, using coupling constants determined in A-dependent vector meson photoproduction,[4] and normalized to $\sigma_{\gamma p}$ below 16 GeV.[5] (Normalization uncertainties are 1.4%.) The same procedure using the (less justifiable) colliding beam coupling constants[4] yields the dashed curve. (Any attempt to normalize to all the data yields a very poor fit,[3] even if, contrary to published systematic uncertainties, one allows separate normalization constants for the two experiments.)

The results imply an excess of 2 to 6 μb. To the extent that the energy dependence of the σ_{Vp}'s used are representative of "old physics," the excess might be due to something new, such as charm. Its value is consistent with a charm-anticharm contribution predicted by several VMD models[6] and by at least one QCD calculation.[7] An alternative, suggested in a contribution to this conference (Gotsman, Silverman and Soni)[8], is that the excess might be due to an increase in the truly pointlike process of high-$p_\perp$ QCD jet production (although their specific prediction is sensitive to the choice of a $p_\perp$ cut, and one can ask whether the total non-charm cross section would show the increase).

B. Solid-Target Measurements

Measurements of photoproduction from nuclei provide another way to study the hadronic behavior of the photon. The particular behavior observed is shadowing. Results can be displayed in terms of

$$\frac{A_{eff}}{A} = \frac{\sigma_{\gamma A}}{A\sigma_{\gamma N}} = \frac{\sigma_{\gamma A}}{A\sigma_{\gamma p} + (A-Z)(\sigma_{\gamma n} - \sigma_{\gamma p})} \qquad (5)$$

A bare (pointlike) photon would have $A_{eff}/A = 1$, while shadowing means that $A_{eff}/A < 1$.

The critical test here of hadronic structure models is provided by the dependence of A_{eff}/A on the photon's energy. Actual calculations are carried out by combining such a model with the Glauber procedure for hadronic interactions in nuclei. Excellent explanations and detailed descriptions of this are available in the review article by Grammer and Sullivan,[2] so I will just make a few qualitative remarks here. For a component of mass M_H, shadowing sets in at an energy $E_\gamma \sim M_H^2 \ell_H$, where the mean free path for H in a nucleus of uniform density n (nucleons per unit volume) is $\ell_H = 1/(n\sigma_{HN})$. At higher energies, the extent of shadowing of this component is determined by the relative size of ℓ_H and the nuclear diameter. In diagonal GVMD using the ρ^0, ω, ϕ and their recurrences, nearly all shadowing should set in well below the energies of the Fermilab experiment. Thus such models generally predict A_{eff}/A fairly flat with E_γ in this region.

The apparatus is shown in Fig. 3. The central counter (C) intercepted energy from noninteracting photons and most e^+e^- pairs. Produced photons of successively larger angles were detected in lead glass arrays G2 and G3, and the 3-layer Pb-scintillator sandwich S1. Other hadrons entered hadrometers K and S3, and sandwiches S2 and S1. G3 was preceeded by a set of multiwire proportional chambers. The hydrogen target (but not solid targets) was surrounded by 4

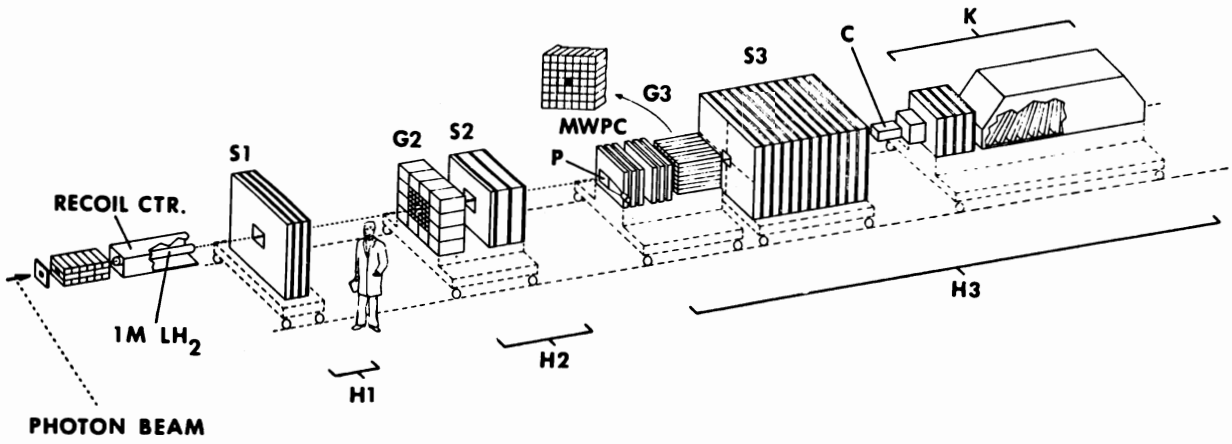

Fig. 3. Apparatus for the Fermilab-Santa Barbara-Toronto experiment, configured for E_o = 90 GeV. Vacuum extended to H3, with helium from the MWPC's to C, the central Pb-scintillator counter. The various hadronic detectors are identified in the text.

recoil counters.[9]

Data were collected for H_2 and Cu at electron beam energies E_o = 40, 60, 90, 135 and 200 GeV, and for C and Pb at 90 GeV. Photons were produced in a radiator 0.0107 or 0.0267 radiation lengths thick, and tagged for E_γ from 45% to 93% of E_o. Target lengths were all close to 0.1 radiation lengths, to keep pair rates about constant. (On Pb, the pair rate is about 3000 times the hadronic cross section.) The three sets of detectors labelled H1, H2 and H3 were independently moveable along the beam, to scale positions roughly with E_o. For nearly all cases, S1 extended to > 90° in the γp center of mass frame. Hadronic events were explicitly detected. The details of hadronic-electromagnetic separation and of the various checks and analysis procedures are available in our publications.[3,10]

Figures 4 - 6 show the cross section results,[10] along with some lower-energy data.[5,11] Systematic uncertainty estimates are +1.3/-0.8% for C and Cu, and +2.4/-1.1% for Pb. To compute A_{eff}/A from Eq. (5) for our data, we have used our hydrogen results (smoothed) for $\sigma_{\gamma p}$, along with the low energy (SLAC) parameterization[5]

$$\sigma_{\gamma p} - \sigma_{\gamma n} = (18.3 \pm 6.1\ \mu b\ GeV^{\frac{1}{2}})/\sqrt{E_\gamma} \ . \qquad (6)$$

Even if this were replaced by 0, most of our results would be changed by < 2%. Fig. 7 shows the results for A_{eff}/A (with all tag bins at each of our E_o's grouped together), consistently defined for all data displayed.[12] The Cu cross section tends to fall in a domain in which $\sigma_{\gamma p}$ rises, resulting in the observed increase of shadowing with energy.

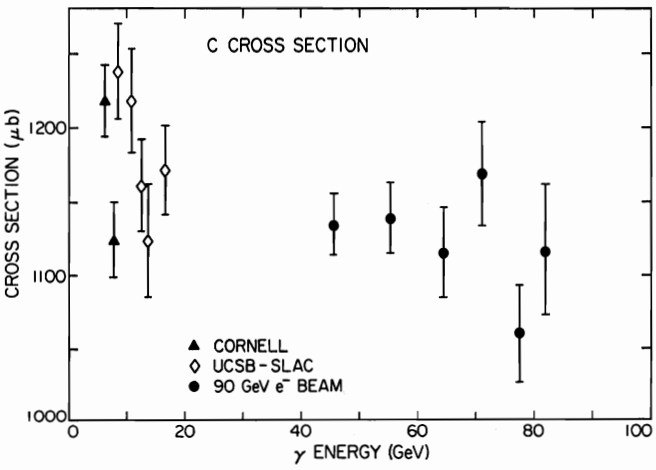

Fig. 4. Hadronic photoproduction cross section from carbon (from Ref. 10, with Cornell and UCSB-SLAC points from Refs. 11 and 5, respectively).

As implied earlier, this contrasts with published VMD models. Fig. 8 is a summary from Grammer and Sullivan[2] of a few of these models, with our points added. The dotted curve is based on Ditsas and Shaw's[13] application of the Fraas-Read-Schildknecht "nearest neighbor" off-diagonal GVMD model, which (aside from its use of a constant nuclear density, as opposed to a Woods-Saxon form) is probably the most complete. Effects like higher mass ($c\bar{c}$ etc.) states and a rising φN cross section would be in the right direction, but seem unlikely to be large enough to produce the observed slope.

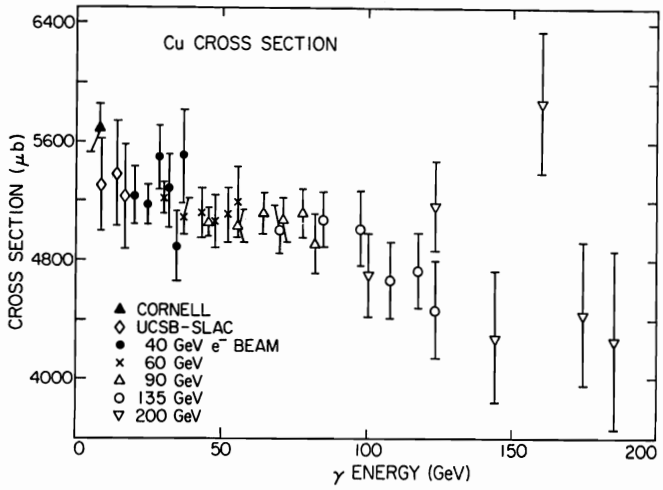

Fig. 5. Hadronic photoproduction cross section from copper.

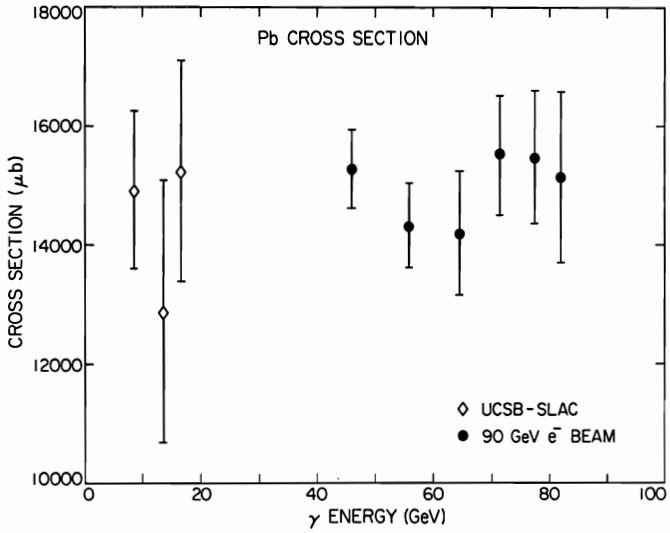

Fig. 6. Hadronic photoproduction cross section from lead.

In hadronic total cross sections from nuclei,[14] a good fit to a Glauber description has seemed to require the inclusion of "inelastic screening",[15] an effect which increases with energy (and tends to increase the amount of shadowing). In forward HA scattering, it involves the dissociation of H to H' at one point inside the nucleus, and its recombination to H at another. In photoproduction, this suggests the importance of off-diagonal GVMD terms, so perhaps the nearest neighbor form does not go far enough. Another possibility to be taken seriously is that the Glauber formalism itself may not be consistent with how hadronic interactions actually occur.[2,16] In any case, this rather muddy ball should now be tossed back to the theorists.

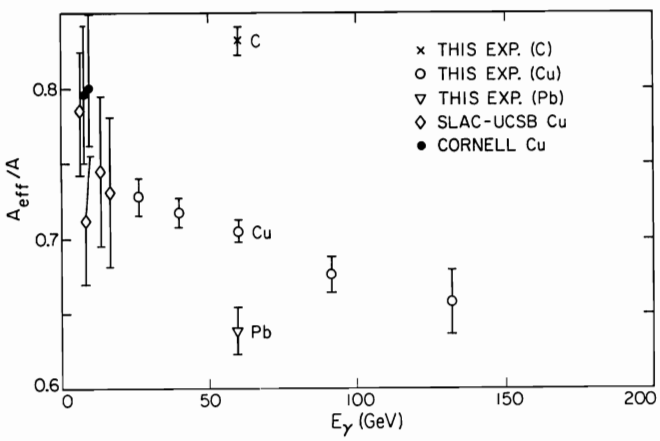

Fig. 7. Energy-dependence of A_{eff}/A.

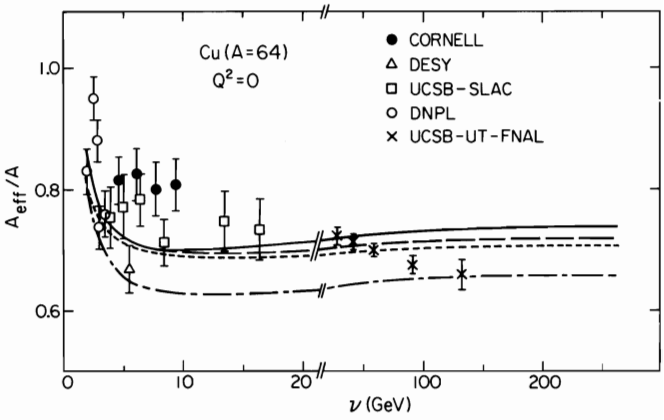

Fig. 8. Comparison of A_{eff}/A measurements with some typical VMD predictions. Curves are from Ref. 2, but the plotted data points have been adjusted for a consistent definition of A_{eff}/A, as per Ref. 12. From top to bottom, curves are: $\rho + \omega + \phi$ + pointlike; diagonal GVMD with Woods-Saxon n; off-diagonal GVMD with constant n; diagonal GVMD with constant n.

III. VECTOR MESON PRODUCTION

A. Electroproduction

I turn next to some recent results on ω and ρ^0 electroproduction from the LAME collaboration at Cornell. The detector is shown in Fig. 9. The data are at $-q^2$ between about 0.8 and 2.6 $(GeV/c)^2$, and W from about 2 to 4 GeV. The events were fully reconstructed, and represent the elastic process:

$$\gamma + p \rightarrow V^0 + p \ .$$

For the ρ^0, a fit was done to separate out not only nonresonant background, but also a small contribution from $\Delta\pi$. Results are presented as virtual photoproduction cross sections in the usual form $\sigma_V = \sigma_T + \varepsilon\sigma_L$ (functions of $Q^2 = -q^2$ and W), where ε for this experiment = 0.75 to 1.0.

Fig. 10 shows the ratio $\sigma_\omega/\sigma_\rho$ vs. Q^2 for several W ranges,[17] along with some results from earlier experiments[18,19] and photoproduction.[20] The relative fractions of diffraction and one-pion exchange in ω photoproduction change considerably between the different W's. The absence of observed Q^2 dependence in the plots leads the LAME group to conclude that the two processes have similar Q^2 dependences to each other and to ρ^0 production.

More detailed studies are possible for the much-studied[18,21,22,23] process of ρ^0 leptoproduction. Data being presented now[24] represent full statistics (twice as much as in the published version[25] and with more complete analysis). The ρ^0 fit used a mass-dependent width and a mass-skewing factor $(M_\rho/M_{2\pi})^n$; n was finally fixed at 1, a value determined by fits to be consistent with all the data.

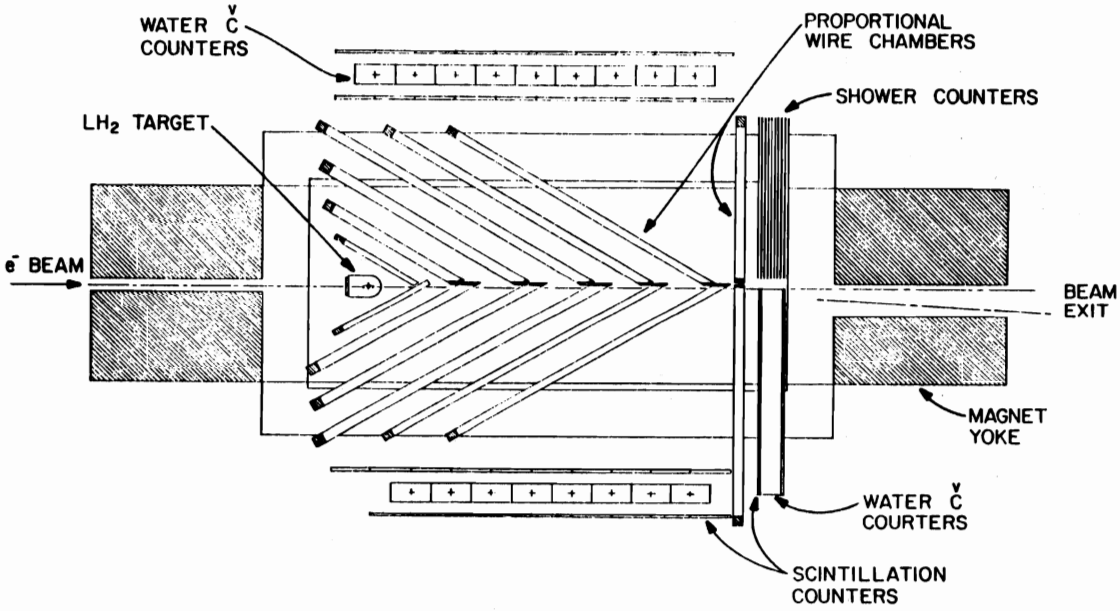

Fig. 9. LAME Detector used in Cornell electroproduction measurements.

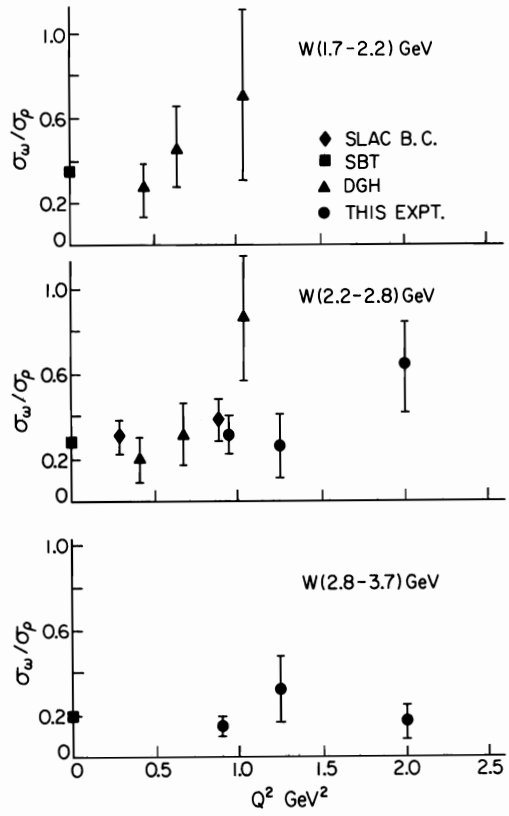

Fig. 10. LAME results on the ratio of ω to ρ^0 electroproduction. Other data are from references 18 (DGH), 19 (SLAC B.C.), and 20 (SBT, photoproduction).

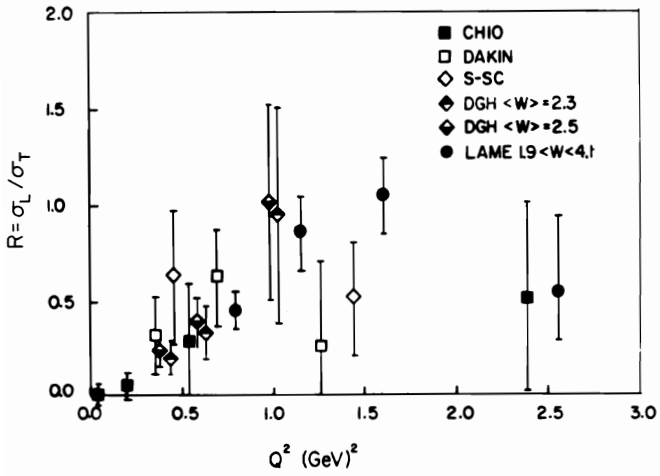

Fig. 11. $R = \sigma_L/\sigma_T$ vs. Q^2 for elastic ρ^0 electroproduction. Shown in addition to LAME data are results from the DESY Streamer Chamber (DGH, Ref. 18), SLAC Streamer Chamber (S-SC, Ref. 21), a SLAC counter experiment (Dakin et al., Ref. 22) and a Fermilab muon experiment (CHIO, Ref. 23).

Fig. 11 shows the ratio $R \equiv \sigma_L/\sigma_T$ vs. Q^2. The LAME results are consistent with no W dependence for $< W > = 2.1$ to 3.5 GeV. It has been customary to represent this ratio in the form $\xi^2 Q^2/M_\rho^2$ with constant ξ^2 (a form suggested by VMD), which is reasonable for $Q^2 \lesssim 1$ (GeV/c)^2. However, it seems likely that this increase does not persist to higher Q^2.

The t distributions have been fit from -0.1 to -0.6 (GeV/c)^2 to an e^{Bt} form. Fig. 12 shows the data for B plotted vs. $\Delta\tau = 1/\Delta E$ (a more exactly calculated form of the Δt in Eq. (1)). Earlier electroproduction data[18,21,22,23] and photoproduction data[20,26,27] are included. The only deviations from constancy are in the region in which this "formation time"[1] is $\lesssim$ the time it takes to traverse the target. There are some discrepancies between the LAME data and DESY Streamer Chamber data.[18] However, their Q^2 ranges overlap, and high-energy data[23] show no Q^2 dependence; so a Q^2 effect could not be concluded at this time.

Fig. 13 shows the new data (and most older data) for $\sigma_T + \varepsilon\sigma_L$ vs. Q^2. There could be 20% relative normalization uncertainties between experiments, so agreement is reasonably good. The LAME data itself shows a decrease with increasing W, but not as much as would have been expected from $Q^2 = 0$ photoproduction and vector dominance.

To make this more quantitative, the LAME group has divided their cross sections by the following VMD form:

$$\sigma(Q^2,W) = \frac{p_\gamma^*(Q^2=0)}{p_\gamma^*(Q^2)}\, e^{B(Q^2,W)[t_{min}(Q^2) - t_{min}(0)]} \cdot \frac{(1+\varepsilon R)}{(1+Q^2/M_\rho^2)^2}\, \sigma(Q^2=0, W) \qquad (7)$$

where p_γ^* is the photon's 3-momentum in the γp c.m. frame. The B values have been taken from LAME mea-

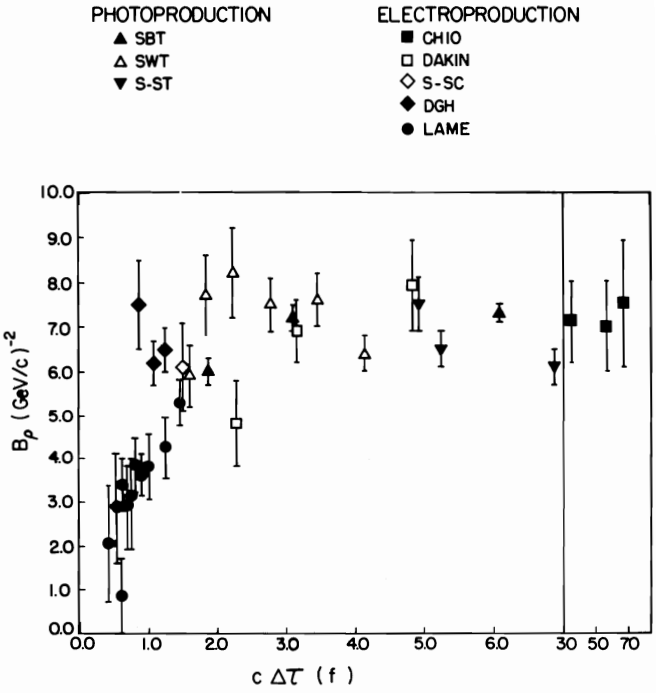

Fig. 12. Slope of t-distribution for elastic ρ^0 electroproduction and photoproduction vs. "formation distance" in fermis. Electroproduction references are as for Fig. 11. Photoproduction data are from references 20 (SBT), 26 (SWT) and 27 (S-ST).

surements (Fig. 12). Based on Fig. 11, a parameterization $R = 0.3\ Q^2/M_\rho^2$ has been used, although this somewhat overestimates the highest Q^2 point. Finally, the real photoproduction data have been parameterized as

$$\sigma\ (Q^2 = 0,\ W) = 9.3 + \frac{30.8}{\nu}\ \mu b.$$

The results are shown in Fig. 14, and imply some disagreement with VMD, especially in W-dependence. (Agreement would be better if $B\sigma$, i.e., the forward cross section, were plotted.) Whether this is due to the low formation times for these data or to some more basic problem remains to be determined. In any case, it seems as if VMD (at least in the form of Eq. (7)) does not well describe what ought to be the simplest electroproduction process for it to deal with.

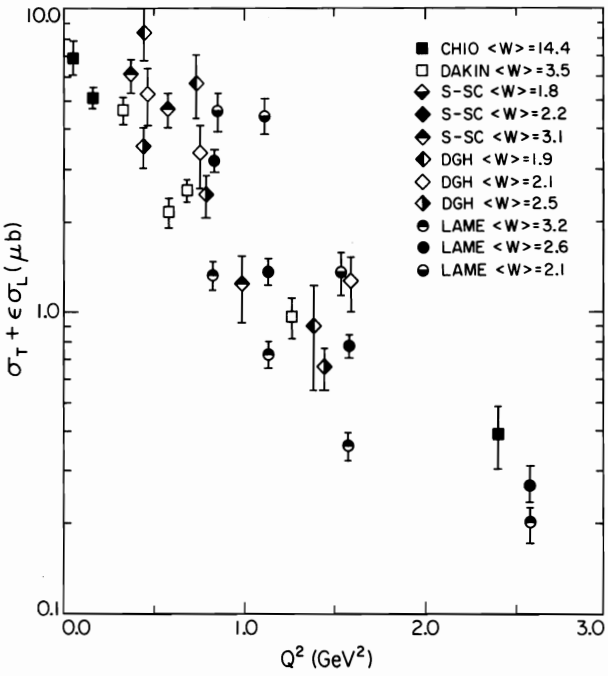

Fig. 13. Elastic ρ^0 electroproduction cross sections. References are as for Figs. 11-12.

B. High-Energy Photoproduction

My last topic will be the high-energy measurements of ρ^0, ω and ϕ photoproduction[28] carried out in Fermilab's Tagged Photon Beam. Here if anywhere VMD should be applicable: Δt is comfortably large; and the GVMD relation

$$f_{\gamma p \to Vp} = \sum_{V'} \frac{e}{2\gamma_{V'}}\ f_{V'p \to Vp} \qquad (8)$$

reduces to a single term in the diagonal model.

The ρ^0 and ϕ were detected via the decays $\pi^+\pi^-$ and K^+K^-, respectively. The apparatus had no magnets or Cerenkov counters. However, our full coverage of the forward c.m. hemisphere allowed selection of candidate events with exactly two tracks and no extra particles. Under these conditions, a plot of the track separation times their total energy (assumed to equal the tagged photon energy) is an excellent substitute for the mass plots we could not make.

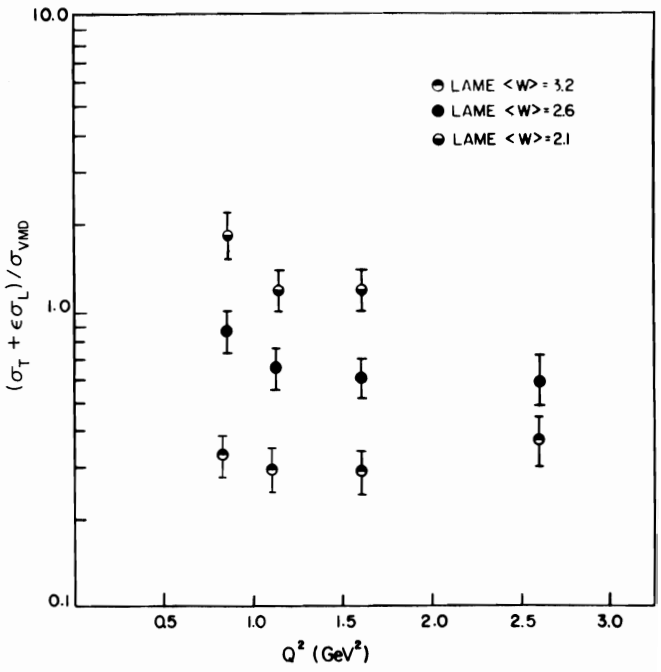

Fig. 14. Ratio of LAME ρ^0 electroproduction cross section to the vector dominance prediction of Eq. (7).

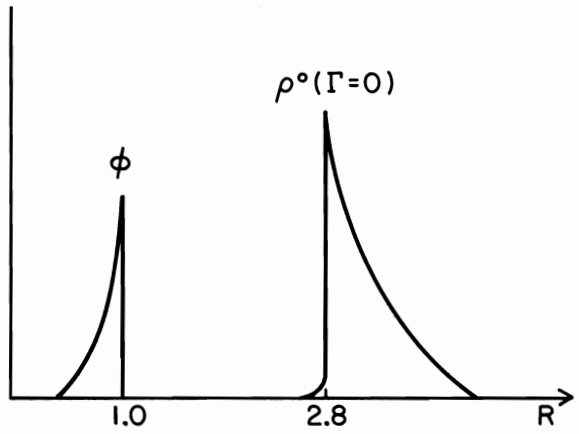

Fig. 15. Idealized distribution (not to scale) of normalized track separation for decays of ϕ and zero-width ρ^0

For a particle of mass M and energy E >> M decaying to two particles of mass $m \neq 0$, the track separation at a distance z from the vertex is given to an excellent approximation by

$$\Delta = \frac{4z\ \sin\theta\ \sqrt{\left(\frac{M}{2}\right)^2 - m^2}}{E\left[\sin^2\theta + \left(\frac{2m}{M}\right)^2 \cos^2\theta\right]} \qquad (9)$$

where θ is the rest frame decay angle.[29] For the ϕ, this has a maximum value

$$\Delta(\phi)_{max} = 0.509\ \frac{z}{E} \qquad (10)$$

(E in GeV), whereas nearly all ρ^0 decays at $M = M_\rho = 0.770$ GeV have $\Delta \geq 1.435\ (z/E)$.

The variable $R \equiv \Delta/\Delta(\phi)_{max}$ eliminates most or all E dependence, and for zero-width ρ^0 and ϕ would have the idealized distribution shown in Fig. 15. In reality, the ρ^0 mass spectrum, geometrical acceptance, target length, beam size, and resolution in both E_γ and Δ all affect this; a typical data plot (target-empty rates subtracted) is shown in Fig. 16.

We fit the data with a Monte Carlo calculation incorporating all those effects. Decays were generated assuming s-channel helicity conservation, and cross sections were assumed $\propto e^{bt}$ with $b(\rho) = 8.5\ GeV^{-2}$ and $b(\phi) = 6.5\ GeV^{-2}$. (Results were insensitive to uncertainties in these numbers.) We included a contribution from e^+e^- pairs in which one member hadronically interacted. (Most of these were suppressed by a cut on electromagnetic energy at very small angles.) For the ρ^0 spectrum we used a Söding parameterization[30] with a mass-dependent width.[31] The fit thus involved the two shape parameters and the amounts of ρ^0, ϕ and e^+e^-. (A small fixed contribution from $\phi \to K_S K_L \to \pi^+\pi^- K_L$ was also allowed for.) The ρ^0 and e^+e^- Monte Carlo curves are included in Fig. 16. The resulting ϕ spectrum with all other processes subtracted is shown in Fig. 17; curves are predictions assuming s-channel helicity conservation (solid) and isotopic decay (dotted).

In addition to correcting for acceptance, decay in flight, inelastic secondary interactions, the ϕ branching ratio, etc.; it was also necessary to correct for events involving target dissociation with no downstream products detected. The key here was that elastic events fire $n \leq 1$ (usually 0) of the four recoil counters, with computable probabilities; whereas inelastic events almost always fire $n \geq 1$ (usually $n \geq 2$). (Probabilities for the latter were estimated using a simple Poisson model in agreement with hadronic studies of target dissociation, and to whose details we are not very sensitive.) The inelastic contamination amounted to 13% of the ρ^0 data and 18% of the ϕ data.

Fig. 18 shows the ρ^0 cross sections along with a sample of older data.[23,32,33] Both ρ^0 and ϕ results have a 5% energy-independent systematic uncertainty; the ρ^0 has an additional 5% uncertainty due to acceptance. Using VMD and quark model relations at

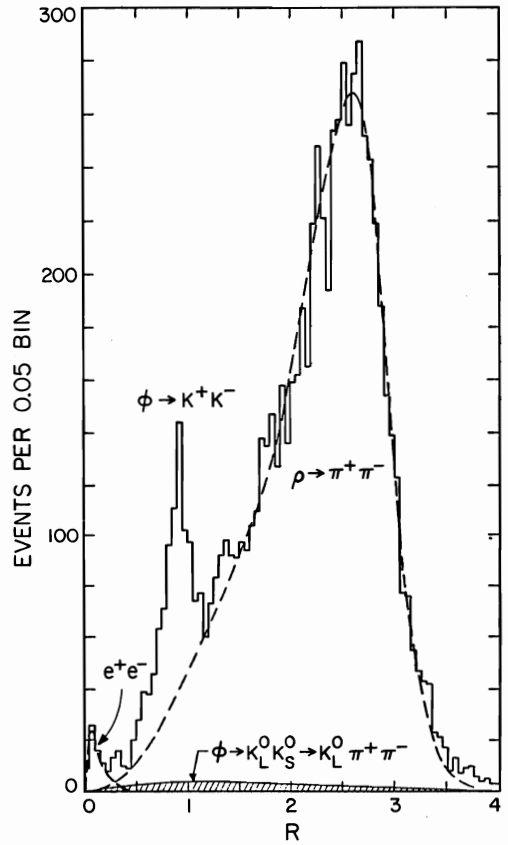

Fig. 16. R distribution for $E_0 = 90$ GeV ρ^0 and ϕ candidates, TPL photoproduction experiment. The curves are discussed in the text.

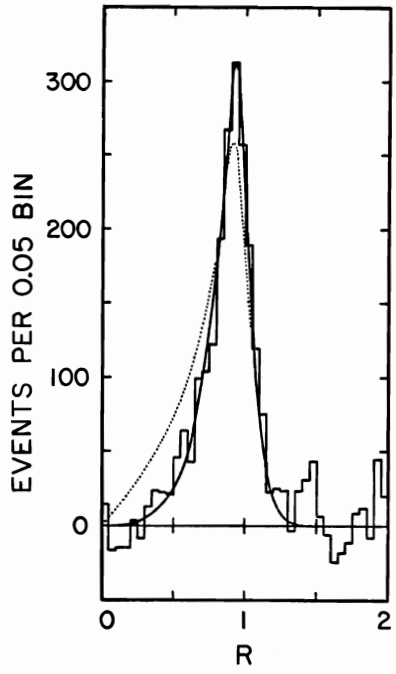

Fig. 17. R distribution for $\phi \to K^+K^-$ obtained by subtracting fits to other processes from the data in Fig. 16. The curves are described in the text.

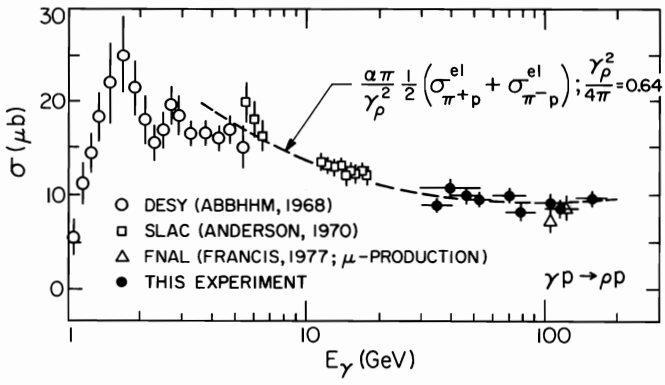

Fig. 18. Energy dependence of the elastic ρ^0 photoproduction cross section. Older data are from references 32, 33 and 23 (top to bottom).

fixed s and t, one can express the cross section in terms of $\pi^{\pm}p$ elastic cross sections:

$$\frac{d\sigma}{dt}(\gamma p\to\rho^0 p) = \frac{e^2}{4\gamma_\rho^2}\left[\frac{p_\pi^*}{2p_\gamma^*}\left(\sqrt{\frac{d\sigma}{dt}(\pi^+p)} + \sqrt{\frac{d\sigma}{dt}(\pi^-p)}\right)\right]^2 \quad (11)$$

where p_X^* = 3-momentum of X in the Xp c.m. frame for the fixed s. A good enough approximation for our purposes is:

$$\sigma(\gamma p\to\rho^0 p) \approx \frac{e^2}{4\gamma_\rho^2}\frac{\sigma(\pi^+p\to\pi^+p) + \sigma(\pi^-p\to\pi^-p)}{2}. \quad (12)$$

This is plotted in Fig. 18 with $\gamma_\rho^2/4\pi = 0.64$, and represents the data well.

Fig. 19 shows the ϕ results, along with lower-energy results[20,32-36] and a curve parameterizing the data shown.[28] Our basic purely experimental result is the rapid rise, which is in accord with the idea that this process may be pure Pomeron. The prediction analogous to Eq. (11) is

$$\frac{d\sigma}{dt}(\gamma p\to\phi p) = \frac{e^2}{4\gamma_\phi^2}\frac{1}{(p_\gamma^*)^2}\left[p_K^*\left(\sqrt{\frac{d\sigma}{dt}(K^+p)} + \sqrt{\frac{d\sigma}{dt}(K^-p)}\right) - p_\pi^*\sqrt{\frac{d\sigma}{dt}(\pi^-p)}\right]^2. \quad (13)$$

We have evaluated $\sigma(\gamma p\to\phi p)$ from this by using forward hadronic data,[37,38] and taking an e^{bt} form for photoproduction with[34] $b(s) = 4.66 + 0.38\ln(s)$. The resulting "data points" have been normalized to the actual photoproduction data, and are shown in Fig. 20 along with the curve (from Fig. 19) representing the photoproduction data. This procedure implies $\gamma_\phi^2/4\pi = 4.7 \pm 0.3$, as compared to 5.5 ± 2.4 from ϕ photoproduction on nuclei (and 2.83 ± 0.2 from colliding beams). The VMD-quark model prediction is seen to be consistent with the energy dependence of the photoproduction data.

For the ω, we utilized the $\pi^0\gamma$ decay mode, and relied on signals in our Pb-glass arrays. (See Fig. 3.) Again, our full coverage was used to select candidate events for having 3 photons and nothing else. Fig. 21a shows all three 2γ mass combinations for each event; Fig. 21b includes only the combination nearest the π^0 mass. A cut on the latter from 80 to 220 MeV leads to the 3γ spectrum of Fig. 22. Properties of events in the ω peak are well simulated by Monte Carlo calculations. The center of mass decay angle distribution for $\omega\to\pi^0\gamma$ corrected for acceptance is shown in Fig. 23, along with the $1 + \cos^2\theta$ prediction of s-channel helicity conservation.

Corrections were applied for acceptance, branching ratio, inelastics, and several small effects. The inelastic contamination here was 26%, larger than for the ρ^0 or ϕ probably because downstream particles could not be as cleanly vetoed. (This is still a reasonable amount, based on lower-energy measurements and also on studies of target dissociation in hadronic reactions.) The correction was checked by requiring that the recoil counter which fired (if any) be opposite the ω. The latter method was also used to exclude inelastic events from t-distributions, shown in Fig. 24 along with fits of the form $d\sigma/dt = Ae^{bt}$. The average $b = 8.42 \pm 0.74\ \text{GeV}^{-2}$. Our values of b are shown with lower-energy results in Fig. 25. The curve is roughly what one would expect from the VMD-quark model relation analogous to Eq. (11) (with γ_ρ replaced by γ_ω).

The integrated $\sigma(\gamma p\to\omega p)$ is shown in Fig. 26. (Systematic uncertainties are about 8%.) The curve is the prediction analogous to Eq. (12), with additional factors of $(p_\pi^*/p_\gamma^*)^2$ and $e^{-b|t_{min}|}$, since we are trying to carry the comparison to low energy. Normalization to the TPL data has been achieved by using $\gamma_\omega^2/4\pi = 5.4 \pm 0.4$. The curve is in agreement with the data if only natural-parity-exchange results (thus excluding the one-pion-exchange process) are used at the low energies.

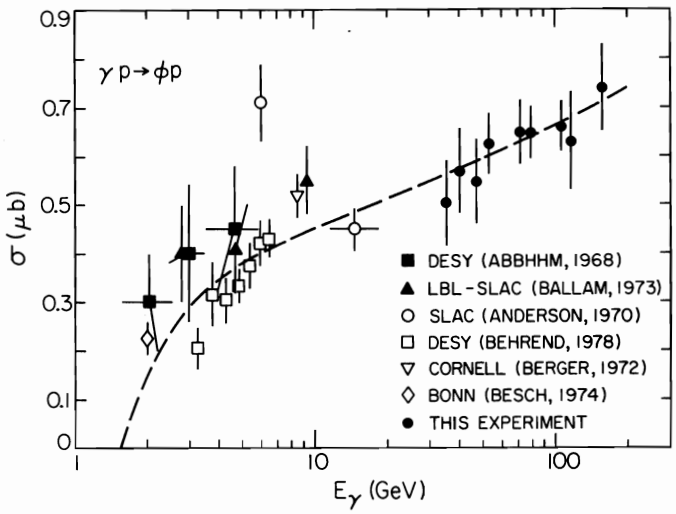

Fig. 19. Energy dependence of the elastic ϕ photoproduction cross section. The symbols listed are, top to bottom, from references 32, 20, 33, 34, 35, 36 and the TPL experiment. The curve is a smooth parameterization of the data.

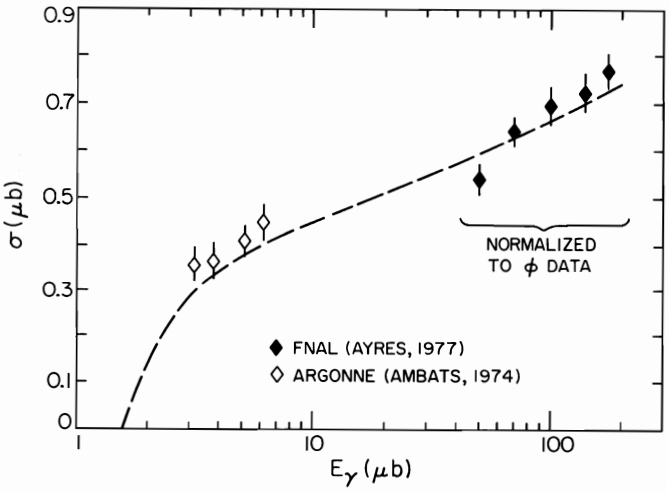

Fig. 20. VMD-quark model predictions (from Eq. 13) for ϕ photoproduction, using data from hadron-beam experiments, and normalized to the TPL photoproduction data. The curve is the same as in Fig. 19, and represents all of the photoproduction data.

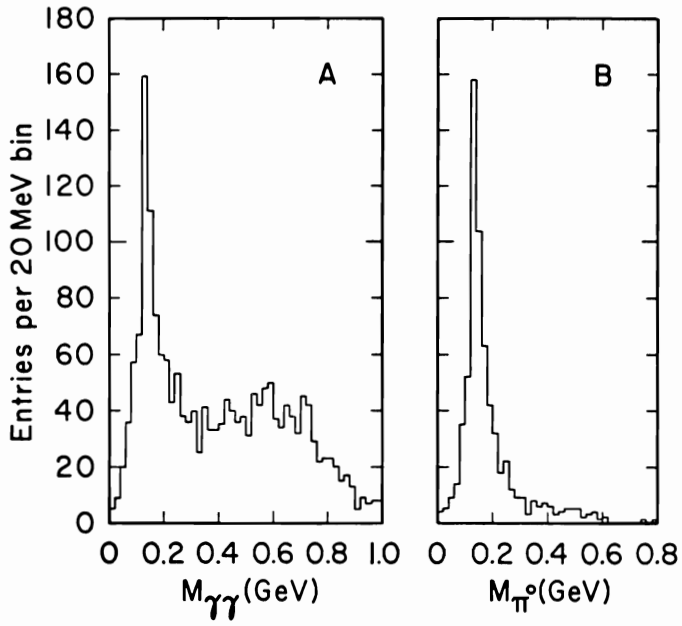

Fig. 21. Two-photon mass spectrum for ω candidates, TPL photoproduction experiment. (a) shows all three combinations for each event. (b) shows only the combination nearest the π^0 mass.

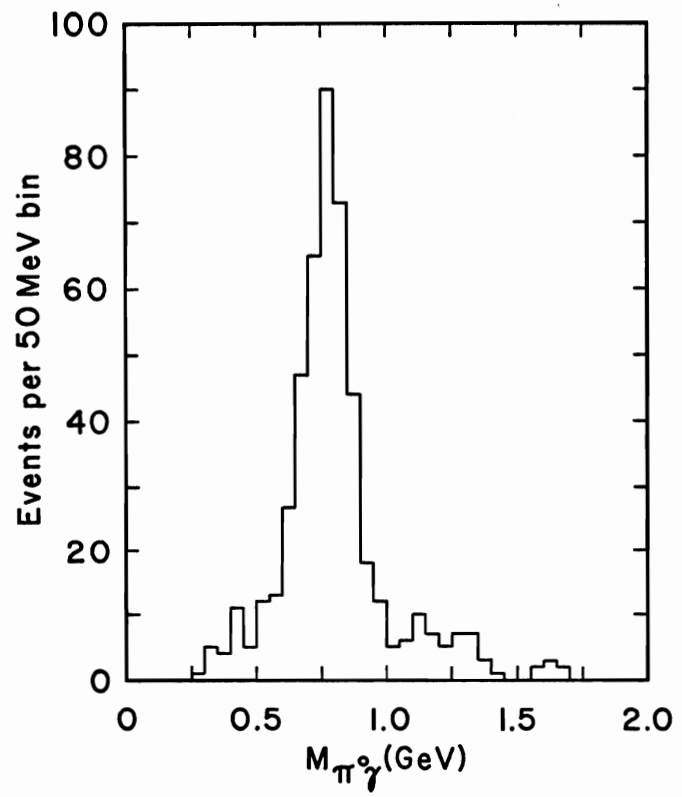

Fig. 22. Three-photon mass distribution for ω candidates passing all analysis cuts, TPL photoproduction experiment.

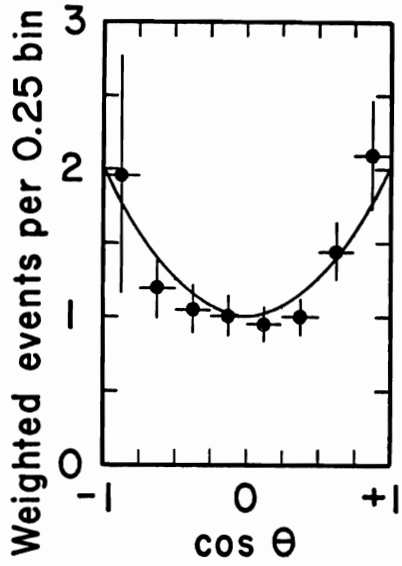

Fig. 23. Decay angle distribution (corrected for acceptance) in the helicity frame for $\omega \to \pi^0\gamma$. The curve is $1 + \cos^2\theta$.

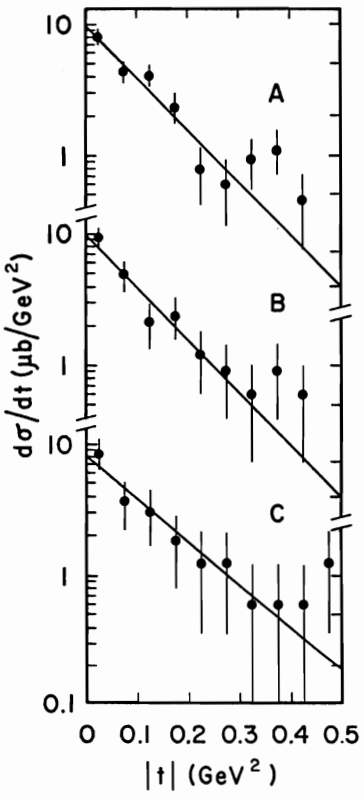

Fig. 24. t distributions and Ae^{bt} fits for elastic ω photoproduction.

Table I summarizes the values of $\gamma_V^2/4\pi$ obtained by normalizing to TPL data, and for comparison the values[4] from "A-dependent photoproduction" (V photoproduction from heavy nuclei) and from $e^+e^- \to V$. I do not want to comment further on the precise values and their significance, because their interpretation

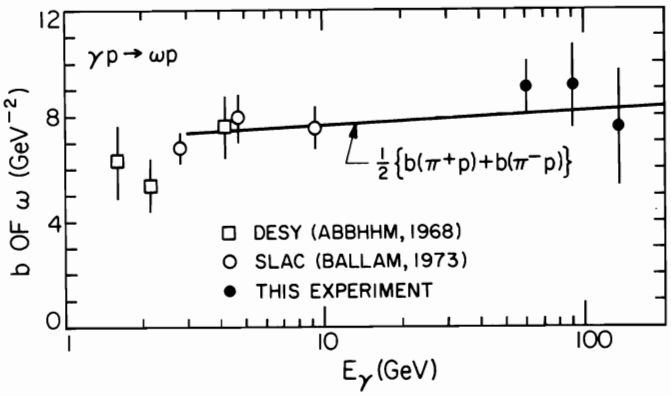

Fig. 25. Slopes (b) of t-distributions for elastic ω photoproduction. DESY and SLAC data are from References 32 and 20.

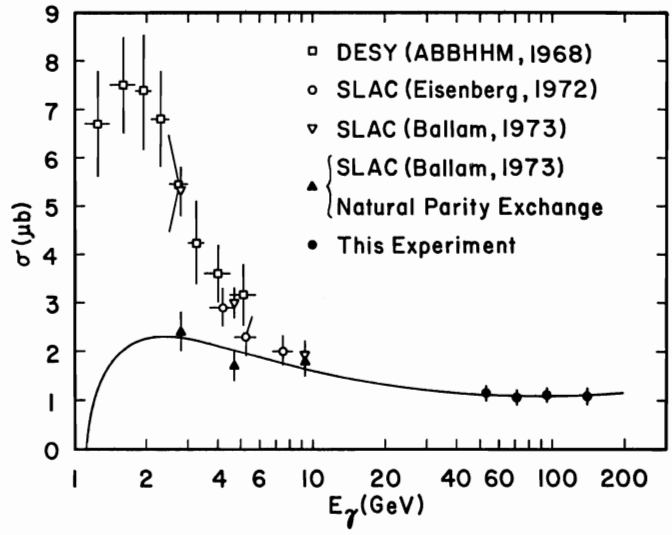

Fig. 26. Energy dependence of the elastic ω photoproduction cross section. The three older experiments are (top to bottom symbols) References 32, 26, and 20; the high energy points are TPL data. The curve is a VMD-quark model prediction. (See text.)

is ambiguous. In particular, the VMD equations used omit off-diagonal contributions (including possible ω-φ mixing).

TABLE I: Values of $\gamma_V^2/4\pi$

V	Normalized to TPL	A-dependent Photoproduction	e^+e^-
ρ^0	0.65 ± 0.03	0.61 ± 0.03	0.64 ± 0.1
ω	5.4 ± 0.4*	7.5 ± 1.3	4.6 ± 0.5
φ	4.7 ± 0.3	5.5 ± 2.4	2.8 ± 0.2

*6.5±0.6 with correction for ρ^0-ω interference

The following conclusions are on firmer ground:

(1) High-energy ρ^0 and ω photoproduction cross sections are flat to within statistics (9 data points, ≈ 5% each for the ρ^0; 4 data points, ≈ 14% each for the ω).

(2) The φ cross section rises rapidly with E_γ (as would be expected for a pure-Pomeron process).

(3) The ω has $d\sigma/dt$ consistent with e^{bt}, with $\langle b \rangle = 8.42 \pm 0.74$ GeV^{-2}.

(4) All three γp → Vp processes have energy dependences consistent with the predictions of VMD plus an additive quark model. Put another way, the energy-dependences of the Vp elastic cross sections extracted from photoproduction data (using VMD) are consistent with those extracted from hadronic data (using the quark model).

ACKNOWLEDGMENTS

This work was supported in part by the U.S. Department of Energy. The results were of course dependent on the contributions of many physicists in the TPL and LAME collaborations (see References 3 and 25). Special thanks go to Roland Egloff whose thesis project was the vector meson photoproduction analysis; and to David Cassel, who made available the recent LAME results.

NOTES AND REFERENCES

(1) T. H. Bauer, R. D. Spital, D. R. Yennie, and F. M. Pipkin, Rev. Mod. Phys. 50, 261 (1978).

(2) G. Grammer and J. D. Sullivan, in Electromagnetic Interactions of Hadrons, II, edited by A. Donnachie and G. Shaw (Plenum, 1978).

(3) D. O. Caldwell, J. P. Cumalat, A. M. Eisner, A. Lu, R. J. Morrison, F. V. Murphy, S. J. Yellin, P. J. Davis, R. M. Egloff, M. E. B. Franklin, G. J. Luste, J. F. Martin, J. D. Prentice, and T. Nash, Phys. Rev. Lett. 40, 1222 (1978).

(4) D. W. G. S. Leith, in Electromagnetic Interactions of Hadrons, II, op. cit.

(5) D. O. Caldwell et al., Phys. Rev. D 7, 1362 (1973).

(6) F. E. Close, D. M. Scott, and D. Sivers, Nucl. Phys. B117, 134 (1976); B. Margolis, Phys. Rev. D 17, 1310 (1978).

(7) F. Halzen and D. M. Scott, Phys. Lett. 72B, 404 (1978). Other QCD calculations yield a smaller result; see, for example, M. A. Shifman et al., Phys. Lett. 65B, 255 (1976).

(8) E. Gotsman, D. Silverman, and A. Soni, contributed paper to this conference.

(9) For further information on the apparatus, see Ref. 3, and also J. P. Cumalat, Thesis, University of California at Santa Barbara (1977, unpublished).

(10) D. O. Caldwell et al., Phys. Rev. Lett. 42, 553 (1979).

(11) S. Michalowski et al., Phys. Rev. Lett. 39, 737 (1977).

(12) See A. M. Eisner, in Particles and Fields-1977, edited by G. H. Thomas, A. B. Wicklund, and P. Schreiner (Amer. Inst. of Physics, 1978).

(13) P. Ditsas and G. Shaw, Nucl. Phys. B113, 246 (1976).

(14) P. V. R. Murthy et al., Nucl. Phys. B92, 269 (1975); J. Biel et al., Phys. Rev. Lett. 36, 1004 (1976); A. Gsponer et al., Phys. Rev. Lett. 42, 9 (1979).

(15) V. A. Karmanov and L. A. Kondratyuk, Pis'ma Zh. Eksp. Teor. Fiz. 18, 451 (1973) [JETP Lett. 18, 266 (1973)].

(16) H. I. Miettinen and J. Pumplin, Phys. Rev. Lett. 42, 204 (1979).

(17) J. T. Linnemann et al., Phys. Rev. Lett. 41, 1266 (1978).

(18) P. Joos et al., Nucl. Phys. B113, 53 (1976).

(19) J. Ballam et al., Phys. Rev. D 10, 765 (1974).

(20) J. Ballam et al., Phys. Rev. D 5, 545 (1972); Phys. Rev. D 7, 3150 (1973).

(21) C. del Papa et al., Phys. Rev. D 19, 1303 (1979).

(22) J. T. Dakin et al., Phys. Rev. D 8, 687 (1973).

(23) W. R. Francis et al., Phys. Rev. Lett. 38, 633 (1977).

(24) Private communications, D. G. Cassel and D. H. White.

(25) L. A. Ahrens, K. Berkelman, D. G. Cassel, C. T. Day, B. G. Gibbard, D. J. Harding, D. L. Hartill, J. W. Humphrey, T. J. Killian, J. S. Klinger, J. T. Linnemann, E. A. Treadwell, and D. H. White, Phys. Rev. Lett. 42, 208 (1979).

(26) Y. Eisenberg et al., Phys. Rev. D 5, 15 (1972).

(27) J. Park et al., Nucl. Phys. B36, 404 (1972).

(28) The ρ^0 and ϕ results have been published since the Symposium: R. M. Egloff, P. J. Davis, G. J. Luste, J. F. Martin, J. D. Prentice, D. O. Caldwell, J. P. Cumalat, A. M. Eisner, A. Lu, R. J. Morrison, S. J. Yellin, and T. Nash, Phys. Rev. Lett. 43, 657 (1979). The ω results have been submitted for publication by the same authors (University of Toronto preprint). Detailed information may be found in R. M. Egloff, Thesis, University of Toronto (1979, unpublished).

(29) The exact form for the lab opening angle δ is

$$\tan\delta = \frac{4\sin\theta\sqrt{\left(\frac{M}{2}\right)^2 - m^2}}{\sqrt{E^2 - M^2}} \cdot \frac{1}{\sin^2\theta + \frac{4m^2}{M^2}\cos^2\theta - \left(1 - \frac{4m^2}{M^2}\right)\frac{M^2}{E^2 - M^2}}$$

which reduces to Eq. (9) when $E \gg M$ and $0 < \tan\delta \ll 1$.

(30) P. Söding, Phys. Lett. 19, 702 (1965); R. Spital and D. R. Yennie, Phys. Rev. D 9, 126 (1974).

(31) J. D. Jackson, Nuovo Cimento 34, 1644 (1964).

(32) ABBHHM Collaboration, Phys. Rev. 175, 1669 (1968).

(33) R. Anderson et al., Phys. Rev. D 1, 27 (1970).

(34) H. J. Behrend et al., Nucl. Phys. B144, 22 (1978).

(35) C. Berger et al., Phys. Lett. 39B, 659 (1972).

(36) H. J. Besch et al., Nucl. Phys. B70, 257 (1974).

(37) I. Ambats et al., Phys. Rev. D 9, 1179 (1974).

(38) D. S. Ayres et al., Phys. Rev. D 15, 3105 (1977).

DISCUSSION

Q. (Eisenberg, Weizmann Inst.) Have you measured ϕ photoproduction forward slopes; and do they shrink?

A. No. The experiment did not have the capability of measuring t distributions for ϕ or ρ because we didn't have individual energy measurements on the two particles. Thus, we didn't have enough resolution to determine adequate t values.

Q. (Weinstein, Northeastern) In your 3γ observation of the ω, do you have an estimate of the magnitude of the $\rho\omega$ interference contribution?

A. We made a very small correction for the $\pi^0\gamma$ decay of the ρ, but our statistics are certainly far too poor to actually observe a real effect there. There are no other processes leading to 3γ final states that we seem to have had enough statistics to measure, as far as I can tell.

Q. (Treadwell, Fermilab) Do you have any data related to recurrences of the ϕ meson or the ω meson?

A. No, not in this experiment; I think that the next speakers will possibly have something to say about them.

Q. (Gotsman, Tel-Aviv) I think in view of your fit to the ϕ photoproduction (finding a value of $\gamma_\phi^2/4\pi = 4.7$), you should remove the curve using the coupling constant (2.8) taken from the colliding beam experiment. You seem to have shown that the A dependent coupling is the right one to use. I think it was the first slide that you showed with two curves in the total photoproduction, the one you should remove now.

A. The purpose of the colliding beam curve (in Fig. 1) was to give an idea of what sort of range of predictions one might get by taking different linear combinations of ρ^0 and ϕ, which is what that really effectively does. The purpose of showing it was only to point out that, in fact, doing that sort of thing could not remove the discrepancy between the prediction and the data. While the solid curve is the more believable one (and now even more so than before), we wanted to state the conclusion--that something new was going on--independent of any specific vector dominance predictions.

Q. (Silverman, Cornell) It seemed to me that the energy dependence of the A-effective for copper was not reproduced in lead. Was that a correct impression or not?

A. I think it has to do more with the scale of the plots. The lead data were over a much narrower energy range than the copper data. One needed the

high energy points at copper to really establish the conclusion of energy dependence. Those data were simply not collected for lead.